Magnetic structure of the quasi-one-dimensional La_{3}OsO_{7} as determined by neutron powder diffraction

Ryan Morrow, Michael A. Susner, Michael D. Sumption, and Patrick M. Woodward

Phys. Rev. B **92**, 134402 — Published 5 October 2015

DOI: 10.1103/PhysRevB.92.134402

Magnetic Structure of the Quasi-One-Dimensional La_3OsO_7 as Determined by Neutron Powder Diffraction

Ryan Morrow,[1] Michael A. Susner,[2,3] Michael D. Sumption,[2] and Patrick M. Woodward[1]

[1]Department of Chemistry and Biochemistry, The Ohio State University, Columbus, Ohio 43210-1185, USA

[2]Department of Materials Science and Engineering, The Ohio State University, Columbus, Ohio 43210-1185, USA

[3]Materials Science and Technology Division, Oak Ridge National Laboratory, Oak Ridge, TN 37831, USA

Abstract

Insulating $5d^3$ La_3OsO_7 and the isostructural hole-doped analog $La_{2.8}Ca_{0.2}OsO_7$ that feature pseudo-one-dimensional zig-zag chains of corner-sharing OsO_6 octahedra have been synthesized and their magnetic and electrical transport properties characterized. Both compounds are insulating antiferromagnets. Long range magnetic order between the antiferromagnetic chains is determined with a propagation vector k = 1/2, 1/2, 1 and T_N = 45 and 33 K for the parent and doped materials. An Os^{5+} moment of 1.7(1) μ_B for La_3OsO_7 and 1.2(2) μ_B for $La_{2.8}Ca_{0.2}OsO_7$ is refined. The long range magnetic structure is compared to the isostructural compounds La_3RuO_7 and La_3MoO_7, both of which adopt different magnetic structures.

Introduction

Materials having quasi-one-dimensional (1D) structures have been widely studied for their interesting electronic and magnetic properties, such as charge density waves [1, 2], spin-Peierls transitions [3, 4], and novel magnetic excitations [5, 6]. While the magnetism of many pseudo-1D structure types containing 3d transition metal ions have been studied [7, 8], quasi-1D oxides containing 5d transition metal ions are much less investigated. Given the decreased electron correlations and increased spin orbit coupling of the 5d oxides the magnetic behavior of such compounds may show important differences with analogous 3d oxides.

One such compound is La_3OsO_7, which adopts a weberite-type structure. Like pyrochlore and bixbyite, the weberite structure can be derived from the fluorite structure by ordering of cations and anion vacancies [9]. In the weberite-type structure adopted by many RE_3MO_7 compositions (*RE* = trivalent rare earth ion, *M* = pentavalent cation) one-third of the rare earth cations are 8-coordinate, two-thirds of the rare earth cations are 7-coordinate, while the *M* cations reside in a 6-coordinate distorted octahedron [10]. The MO_6 octahedra share opposite corners to form infinite zig-zag chains that run parallel to the *c* axis, as shown in Figure 1. The buckling of the MO_6 results in *M*□O□*M* angles of approximately 145° along the chain axis. Members of the

RE_3MO_7 family include $RESbO_7$ [11], $RENbO_7$ [11, 12], $REMoO_7$ [13], $RERuO_7$ [14-16], $RETaO_7$ [11], $REReO_7$ [17, 18], $REOsO_7$ [19-22], and $REIrO_7$ [23, 24], which collectively represents a considerable degree of chemical diversity. Possibly due to the zig-zag configuration of the octahedral chains, the electrons are localized on the *M* cation and therefore prime candidates for one-dimensional magnetic behavior. The wide variety of cations that can be incorporated in this system provides an opportunity to study one-dimensional magnetism with electron configurations on the transition metal ion that range from d^1 to d^4. It is to be noted that additional polymorphs with Ln_3MO_7 stoichiometry exist, though these materials are monoclinic and structurally unrelated, having isolated MO_6 octahedra [23, 25].

While many previous reports have included studies of magnetic or structural transitions in these compounds via magnetic susceptibility or X-ray diffraction measurements, relatively little work has been done with neutron diffraction to elucidate the magnetic structures of RE_3MO_7 compounds. In the spin 3/2 compound La_3RuO_7, an ideal candidate for the study of the quasi-one-dimensional magnetism due to the presence of a non-magnetic rare earth cation, Khalifah *et al.* [26] reported evidence of magnetic neutron scattering at low temperatures. Though these data indicated the presence of long range magnetic order, they were not able to determine the magnetic structure. In the 5d analogue La_3OsO_7, Lam *et al.* [19] reported magnetic susceptibility data that differed considerably from that of La_3RuO_7, suggesting the two isoelectronic compounds may have different magnetic structures. However, neutron diffraction studies were not carried out. Here we report a neutron diffraction study of the crystal and magnetic structure of La_3OsO_7, as well as investigate the effects of hole doping through calcium substitution on the lanthanum site.

Experimental

Polycrystalline samples of a maximum size of 1.6 g were prepared by combining La_2O_3 (99.99%, GFS, dried overnight at 1000°C prior to use) and Os metal (99.98%, Alfa Aesar) in an alumina vessel which was sealed in an evacuated silica tube (volume of approximately 40 mL with 3 mm thick walls) along with a secondary crucible containing PbO_2 which served as a sacrificial O_2 source at elevated temperatures. The reaction is thus described as:

$$1.675\ La_2O_3 + Os + (3\ PbO_2) \rightarrow La_3OsO_7 + (3\ PbO) + 1/4\ O_2 + 0.175\ La_2O_3$$

$$1.575\ La_2O_3 + 0.2\ CaO + (3.1\ PbO_2) \rightarrow La_{2.8}Ca_{0.2}OsO_7 + (3.1\ PbO) + 1/4\ O_2 + 0.175\ La_2O_3$$

In accordance with previous work on La_3RuO_7 [14], a calculated excess of La_2O_3 was used in order to prevent the formation of La deficient La-Os-O secondary phases. Although this was not reported to be necessary in the previous report of La_3OsO_7 [19], here it was found to be useful, particularly in the doped case. A calculated excess of PbO_2 was used in order to fully oxidize the target phase. Preparations were heated to 1000 °C for a period of 48 hours in a box furnace located in a fume hood. Care must be taken when heating osmium or osmium-containing

compounds due to the potential formation of toxic volatile OsO_4. Additional care must be taken when evolving gas *in situ*, as tube rupture may occur.

Phase purity was verified via X-ray powder diffraction with a Bruker D8 Advance laboratory diffractomer equipped with a Ge (111) monochromator. Neutron powder diffraction data was collected at Oak Ridge National Laboratory's Spallation Neutron Source (SNS) on the POWGEN [27] beamline with samples sizes of 1.561 g for La_3OsO_7 and 1.531 g for $La_{2.8}Ca_{0.2}OsO_7$. Data were collected using the orange cryostat sample environment with 6 mm vanadium sample cans using chopper settings and wavelength ranges corresponding to bank 2 (0.2760–4.6064 Å) and bank 5 (2.2076–15.3548 Å). Data were collected for 4 hours at each measurement temperature – 5, 30, 70 and 300 K for La_3OsO_7 and 5, 25, 45, 70 and 300 K for $La_{2.8}Ca_{0.2}OsO_7$. Rietveld analysis was conducted using the software package GSAS EXPGUI [28, 29] on both banks simultaneously. Representational analysis was performed with SARAh [30], and magnetic form factor coefficients for Os were adapted from Kobayashi *et al.* [31].

Conductivity measurements were collected using a Quantum Design PPMS with a 4 point contact geometry on sintered bar shaped pellets. Data were collected with zero applied field between the temperatures 300 K and 150 K, below which the samples became too resistive to measure accurately. Magnetic measurements were conducted on Quantum Design SQUID MPMS using loose polycrystalline powders in the temperature ranges 2 to 400 K under an applied field of 1 kOe with FC (1 kOe) and ZFC conditions upon warming.

Results

The neutron powder diffraction data were able to be fit readily with the *Cmcm* spacegroup, using the starting model that had previously been determined [19]. This crystal structure, which has been previously described [14], is shown in Figure 1 and consists of chains of OsO_6 octahedra connected at transverse corners running parallel to the *c* axis. The chains are significantly buckled, with Os−O−Os bond angles along the chain axis of approximately 146−147°. The distance between Os cations in neighboring chains is approximately 6.75 Å. Next nearest neighboring chains are separated by distances equivalent to the *a* and *b* lattice parameters, approximately 7.5 and 11.2 Å, respectively. The refined fit to the neutron diffraction data is shown in Figure 2. Detailed refined structural parameters are available in Tables 1 and 2 for La_3OsO_7 and $La_{2.8}Ca_{0.2}OsO_7$ respectively. Refined anisotropic displacement parameters are reported in Ref. [32].

There is also evidence of the successful doping of calcium into the structure from the neutron powder diffraction data analysis. While the size of the Ca^{2+} is similar to that of La^{3+}, it is slightly smaller (1.12 versus 1.16 Å) [33], explaining the small decrease in the unit cell volume of the doped compound with respect to pure La_3OsO_7. Further evidence for calcium incorporation comes from the refined weight percentages of the La_2O_3 impurity, which was added as a reagent with a predetermined excess, of 7.5(2) and 8.1(2)% for the parent and doped compound,

respectively. These values are in close agreement with the values expected given the initial excesses used (7.3 and 7.5%). No additional phases were present in either diffraction pattern. The occupancies were set to reflect the expected Ca content randomly distributed over both La sites. Attempts to refine the occupancies of these sites did not result in measureable improvement to the fit.

The electrical conductivity of the sintered polycrystalline pellets, shown in Figure 3, displays clear insulating behavior with an increase in resistivity of approximately three orders of magnitude in the temperature range 150 to 300 K. There is a decrease in resistivity of approximately one half of an order of magnitude in the $La_{2.8}Ca_{0.2}OsO_7$ sample; however, the insulating behavior remains intact. The log of the resistivity is shown to be linear when plotted on a $T^{-1/2}$ temperature scale, in accordance with a variable range hopping model [34] with a dimensionality of one ($T^{-1/(1+d)}$ where d is the dimensionality) with an R^2 of 0.9999. Although the data range being fit is not exhaustive, there is a noticeable preference to this model with respect to a simple activated model (T^{-1}; $R^2 = 0.9985$) or a 3D variable range hopping model ($T^{-1/4}$; $R^2 = 0.9991$). The 1D variable range hopping mechanism can be easily rationalized given the one-dimensional nature of the isolated corner sharing OsO_6 chains.

The temperature dependence of the magnetization of both compounds is shown in Figure 4. For La_3OsO_7 a broad feature near 100 K can be attributed to intrachain one-dimensional magnetic correlations. Although this feature is not as clear as has been previously shown [19], it is visible as a deviation from Curie-Weiss behavior. The very sharp cusp at 45 K is due to three dimensional magnetic ordering; an additional broad feature centered at 12 K is noted. All three features are consistent with the observations of Lam *et al.* [19]. The temperature dependent magnetization of $La_{2.8}Ca_{0.2}OsO_7$ has similar features as well, including a broad maximum near 90 K due to the intrachain correlations, a sharp feature at 33 K likely due to three dimensional ordering, and an additional feature at 19 K.

Both data sets could be fit to a Curie-Weiss law in the temperature range 200 – 400 K, further confirming the concept of localized magnetic moments. Effective moments of 3.14 and 2.80 μ_B and Weiss constants of −204 and −211 K were calculated for the parent and doped material, respectively. The reduced effective moment seen in the $La_{2.8}Ca_{0.2}OsO_7$ sample is consistent with calcium doping leading to an increase in the oxidation state of osmium (from Os^{5+} to $Os^{5.2+}$), and corresponding decrease in the number of unpaired electrons per osmium. In both samples effective moments are reduced from the theoretical spin only value of 3.87 μ_B, presumably due to the effects of spin orbit coupling. Interestingly, Lam *et al.* [19] performed a similar analysis with data collected up to 600 K, showing that the slope of the inverse magnetic susceptibility changed at high temperatures resulting in an effective moment equal to the theoretical spin-only value, within experimental error.

In La_3OsO_7 several magnetic reflections appear in the neutron powder diffraction patterns collected at 30 and 5 K, below the presumed 3D ordering temperature of 45 K (Figure 5). The

two strongest magnetic reflections could be indexed as the (1/2, 1/2, 1) and (3/2, 1/2, 1) reflections, indicating a propagation vector of **k** = 1/2, 1/2, 1. Representational analysis using SARAh yielded two potential irreducible representations which dictated the orientation of the Os moments and coupling to neighboring Os moments within a given chain. The output of the SARAh program is given in Ref. [32]. Γ(1) contained basis vectors which would allow neighboring spins within a chain to have antiferromagnetically coupled components within the *ab* plane and ferromagnetically coupled *c* components. Γ(3) contained basis vectors which would allow neighboring spins within a chain to have ferromagnetically coupled components within the *ab* plane and antiferromagnetically coupled *c* components.

Attempts at fitting both of these possibilities showed unequivocally that Γ(1) was the correct choice. The inclusion of a ferromagnetic component parallel to the *c* axis did not improve the refinements nor is it consistent with the previously described magnetization measurements. It was therefore fixed at zero. The refinement of this model had some sensitivity to the orientation of the moments within the *ab* plane with the best fit corresponding to a structure where the moments are tilted by 20-30 degrees from the *a* axis, approximately in the direction of the nearest neighbor chain along the face diagonal (approximately 33.8 degrees away from the *a* axis). A representation of the collinear magnetic structure is shown in Figure 6. In addition to the antiferromagnetic coupling along the chain direction, each Os moment has an antiferromagnetic alignment with Os spins in two of the four nearest neighbor chains, and a ferromagnetic alignment with the other two.

At the lowest temperature measured, the magnetic moment refined on Os^{5+} was 1.7(1) μ_B. This number is significantly reduced from the expectation of a magnetic ion with 3 unpaired electrons. However, the result is in excellent agreement with several recent neutron diffraction studies in Os^{5+} bearing double perovskites [35, 36] where the moment is found to be reduced primarily due to the effects of covalency in the Os−O bonds. While calculations indicate the Os moment is reduced primarily through covalency with oxygen, a small reduction due to spin-orbit coupling is also permitted [36, 37]. There did not appear to be any substantial change in the magnetic structure between 5 and 30 K that would give some clues about the origin of the lower temperature (12 K) feature in the magnetic susceptibility data. There is a small increase in the intensity of the (1/2, 1/2, 1) peak relative to (3/2, 1/2, 1) which may correspond to a slight reorientation of the moment in the *ab*-plane as the refined moment angle suggests, but the refinement was not sensitive enough to definitively link this subtle change with the feature in the susceptibility data.

In considering the magnetic structure refinement of the hole doped $La_{2.8}Ca_{0.2}OsO_7$, there were no obvious features in the low temperature neutron diffraction data to suggest that the nature of the magnetic structure had changed from the parent compound, save for an overall reduction in intensity of the magnetic scattering presumably resulting from a reduction in the number of unpaired electrons from 3 to 2.8. The moment refined on Os was 1.2(2) μ_B at 5 K which is a greater reduction in moment than might be expected from the absence of 0.2 electrons per Os.

As was the case for La_3OsO_7, there was no clear change in the observed neutron scattering between 5 and 25 K that could be used to shed light on the nature of the 19 K feature observed in the magnetization data. The neutron diffraction data are consistent with the assignment of the 33 K transition as the three dimensional ordering transition. For both materials, broad but weakened magnetic scattering intensity can be seen in the diffraction patterns collected at temperatures just above the sharp three dimensional ordering transitions, presumably due to short range interchain correlations.

It is instructive to consider the magnetic structure of La_3OsO_7 in the context of prior magnetic neutron scattering work on this family of compounds. In the isoelectronic material La_3RuO_7, only two magnetic reflections were observed [26] with d spacings of 9.80 Å and 12.20 Å. These positions do not correspond to the scattering which would result from the magnetic structure of La_3OsO_7. In fact, one must at least quadruple the unit cell in all three dimensions to find possible indices of the peaks observed in La_3RuO_7. These deviations indicate that the magnetic structure of La_3RuO_7 is most certainly different than what is found for La_3OsO_7 studied here, as had been predicted [19]. In the study of the d^1 La_3MoO_7 [13], a small increase in the intensity of several nuclear peaks was observed and attributed to a 3D ordered magnetic structure, presumably with a propagation vector of **k** = 0, 0, 0. This intensity was fit with a model wherein nearest-neighbor antiferromagnetic chains are antiferromagnetically ordered, which does not require an expansion of the unit cell to describe. Using this language, the magnetic structure of La_3OsO_7 could then be described as an antiferromagnetic ordering of the next-nearest-neighbor chains. It is remarkable that three distinct 3D magnetic structures appear to have been observed in these three compounds with electronic configurations of $4d^1$, $4d^3$, and $5d^3$ and nonmagnetic La^{3+} cations. Furthermore, it has been observed in the $4d^3$ cases of Nd_3RuO_7 and Pr_3RuO_7 that ordering schemes corresponding to nearest neighbor AFM Ru chain ordering [38] and an as-yet-unsolved magnetic structure with a propagation vector **k** = 1/2, 1/2, 1/2 are possible [39], indicating that a magnetic rare earth cation can affect the magnetic structure of the chains in a substantial way. It would be interesting to further understand how additional electronic configurations in the La_3MO_7 family might order, what the true magnetic structure of La_3RuO_7 is, and how the addition of a magnetic Ln cation affects the long range magnetic ordering of the chains.

In conclusion, the 3D ordered magnetic structure of the quasi-one-dimensional La_3OsO_7 compound has been determined. The d^3 Os^{5+} ions couple antiferromagnetically along the 1D corner connected chains, but interestingly the interchain coupling is only antiferromagnetic to two of the four nearest neighbor chains. The interchain coupling to more distant chains along the *a* and *b* axes are antiferromagnetic leading to a propagation vector of **k** = 1/2, 1/2, 1. Hole doping, achieved by partially replacing La^{3+} with Ca^{2+}, does not have a remarkable impact on the magnetic or electrical properties.

Author Information

Corresponding Author

Morrow.176@osu.edu

Notes

The authors declare no competing financial interest.

Acknowledgements

Support for this research was provided by the Center for Emergent Materials an NSF Materials Research Science and Engineering Center (DMR-0820414). Additional support was provided by the U.S. Department of Energy, Office of High Energy Physics under Grant Number DE-FG02-95ER40900. A portion of this research was carried out at Oak Ridge National Laboratory's Spallation Neutron Source, which is sponsored by the U.S. Department of Energy, Office of Basic Energy Sciences. The authors thankfully acknowledge Pamela Whitfield for experimental assistance with POWGEN data collection.

References

1) M. Hase, I. Terasaki, and K. Uchinokura, Phys. Rev. Lett. **70**, 3651 (1993).
2) Y. Fujii, H. Nakao, T. Yosihama, M. Nishi, K. Nakajima, K. Kakurai, M. Isobe, Y. Ueda, and H. Sawa, J. Phys. Soc. Jpn. **66.2**, 326-329 (1997).
3) P. Monceau, N. P. Ong, A. M. Portis, A. Meerschaut, and J. Rouxel, Phys. Rev. Lett. **37**, 602 (1976).
4) J. P. Pouget, C. Noguera, A. H. Moudden, and R. Moret, Journal de Physique **46(10)**, 1731-1742 (1985).
5) H.-J. Mikeska and A. K. Kolezhuk. Lect. Notes Phys. **645**, 1 (2004).
6) D. A. Tennant, R. A. Cowley, S. E. Nagler, and A. M. Tsvelik, Phys. Rev. B **52**, 13368 (1995).
7) H. Park, R. Lam, J. E. Greedan, and J. Barbier, Chem. Mater. **15**, 1703-1712 (2003).
8) S. H. Irons, T. D. Sangrey, K. M. Beauchamp, M. D. Smith, and H.-C. zur Loye. Phys. Rev. B **61**, 11594 (2000).
9) J. G. Allpress and H. J. Rossell. J. Solid State Chem. **27**, 115 (1979).
10) G. King, C. M. Thompson, J. E. Greedan, and A. Llobet. J. Mater. Chem. 1, 10487-10494 (2013).
11) L. Cai and J. C. Nino. Acta Cryst. B 65, 269-290, (2009).
12) A. Kanh-Harari, L. Mazerolles, D. Michel, and F. Robert. J. Solid State Chem. **116**, 103 (1995).
13) J. E. Greedan, N. P. Raju, A. Wegner, P. Gougeon, and J. Padiou. J. Solid State Chem. **129**, 320 (1997).
14) P. Khalifah, Q. Huang, J. W. Lynn, R. W. Erwin, and R. J. Cava. Mater. Res. Bull. **35**, 1-7 (2000).
15) D. Harada and Y. Hinatsu. J. Solid State Chem. **158(2)**, 245-253 (2001).
16) D. Harada and Y. Hinatsu. J. Solid State Chem. **164(1)**, 163-168 (2002).

17) G. Wltschek, H. Paulus, I. Svoboda, H. Ehrenberg, and H. Fuess. J. Solid State Chem. **125**, 1 (1996).
18) M. Wakeshima and Y. Hinatsu. J. Solid State Chem. **179(11)**, 3575-3581 (2006).
19) R. Lam, F. Wiss, J. E. Greedan. J. Solid State Chem. **167**, 182-187 (2002).
20) W. R. Gemmill, M. D. Smith, Y. A. Mozharivsky, G. J. Miller, and H.-C. zur Loy. Inorg. Chem. **44**, 7047-7055 (2005).
21) Y. Hinatsu and Y. Doi. J. Solid State Chem. **198**, 176-185 (2013).
22) J. R. Plaisier, R. J. Drost, and D. J. W. Ijdo. J. Solid State Chem. **167**, 182 (2002).
23) R. C. Severance, A. H. Fox, S. J. Mugavero III, M. D. Smith, and H.-C. Zur Loye. J. Chem. Crystallogr. **41**, 496-501 (2011).
24) J. F. Vente and D. J. W. Ijdo. Mater. Res. Bull. **26**, 1255 (1991).
25) P. Khalifah, D. M. Ho, Q. Huang, and R. J. Cava. J. Solid State Chem. **165(2)**, 359-362 (2002).
26) P. Kalifah, R. W. Erwin, J. W. Lynn, Q. Huang, B. Batlogg, and R. J. Cava. Phys. Rev. B **60**, 9573 (1999).
27) A. Huq, J. P. Hodges O. Gourdon, and L. Heroux. Zeitschrift für Kristallographie Proceedings, **1**, 127-135 (2011).
28) A. C. Larson and R. B. Von Dreele. Los Alamos National Laboratory Report LAUR 86-748 (2000).
29) B. H. Toby. J. Appl. Cryst. **34**, 210-213 (1991).
30) A. Wills. Physica B. **276**, 680-681 (1991).
31) K. Kobayashi, T. Nagao, and M. Ito. Acta Crys. A **67**, 473-480 (1991).
32) See Supplemental Material at [URL will be inserted by publisher] for a refined bank 5 diffraction pattern, refined anisotropic displacement parameters, a magnetic scattering figure for $La_{2.8}Ca_{0.2}OsO_7$, and the SARAh output.
33) R. D. Shannon. Acta Cryst. A **32**, 751-767 (1976).
34) N. F. Mott. Phil. Mag. **19**, 835 (1969).
35) A. K. Paul, A. Sarapulova,P. Adler, M. Reehuis, S. Kanungo, D. Mikhailova, W. Schnelle, Z. Hu, C. Kuo, V. Siruguri, S. Rayaprol, Y. Soo, B. Yan, C. Felser, L. H. Tjeng, and M. Jansen. Z. Anorg. Allg. Chem. **641**, 197 (2015).
36) A. E. Taylor, R. Morrow, D. J. Singh, S. Calder, M. D. Lumsden, P. M. Woodward and A. D. Christianson. Phys. Rev B **91**, 100406(R) (2015).
37) H. Matsuura and K. Miyake, J. Phys. Soc. Jpn. **82**, 073703 (2013).
38) D. Harada, Y. Hinatsu, and Y. Ishii. J. Phys.: Condens. Matter **13**, 10825 (2001).
39) F. Wiss, N. P. Raju, A. S. Wills, and J. E. Greedan. Int. J. Inorg. Mater. **2**, 53-59 (2000).

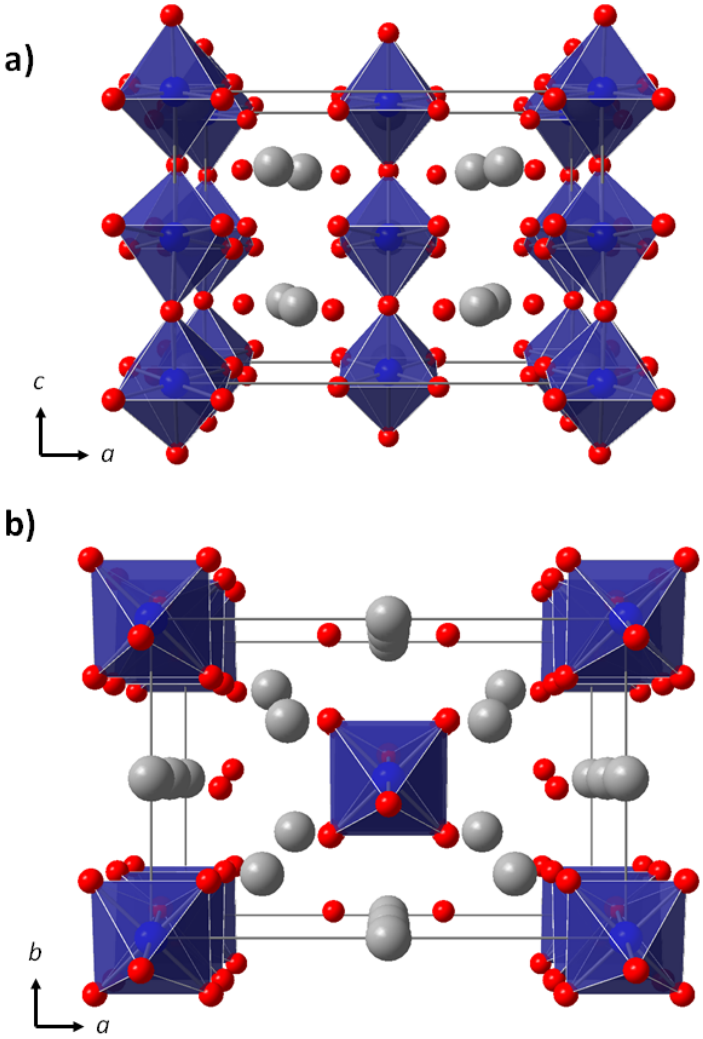

FIG. 1 (color online). Crystal structure of La_3OsO_7 shown with views a) down the *b* axis and b) down the *c*. Os cations are shown as blue spheres within the blue octahedra, La cations are shown as grey spheres, and O anions are shown as red spheres.

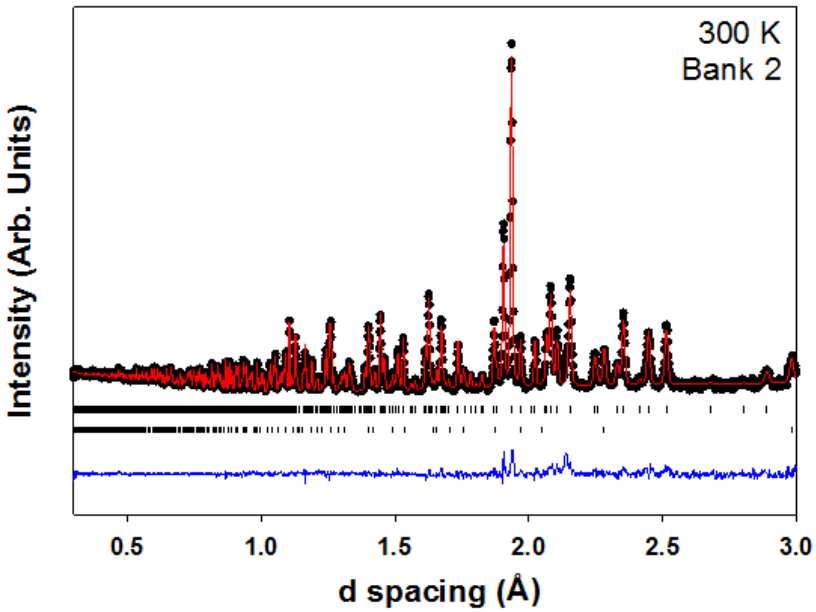

FIG. 2 (color online). Refined neutron powder diffraction data for La_3OsO_7 at 300 K. Black symbols, red curves, and blue curves represent the observed data, calculated pattern, and difference respectively. The upper and lower sets of hash marks signify the main phase and excess La_2O_3 impurity, respectively.

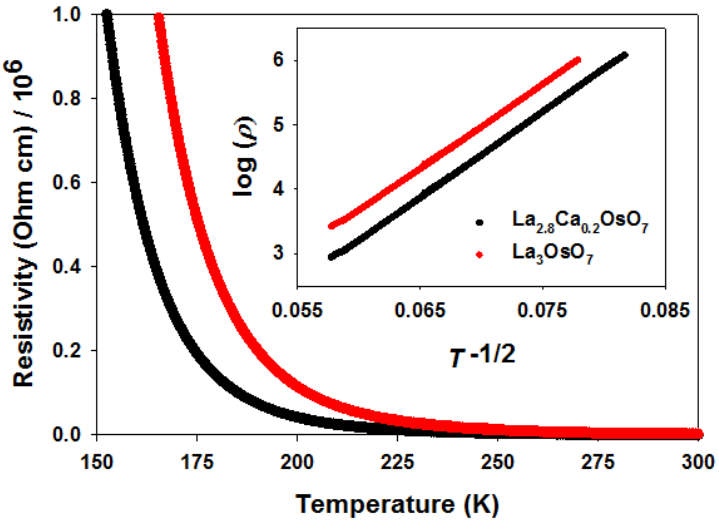

FIG. 3 (color online). The temperature dependence of the electrical resistivity of La_3OsO_7 (black) and $La_{2.8}Ca_{0.2}OsO_7$ (red). The inset shows the linear relationship on a $T^{-1/2}$ scale as described in the text.

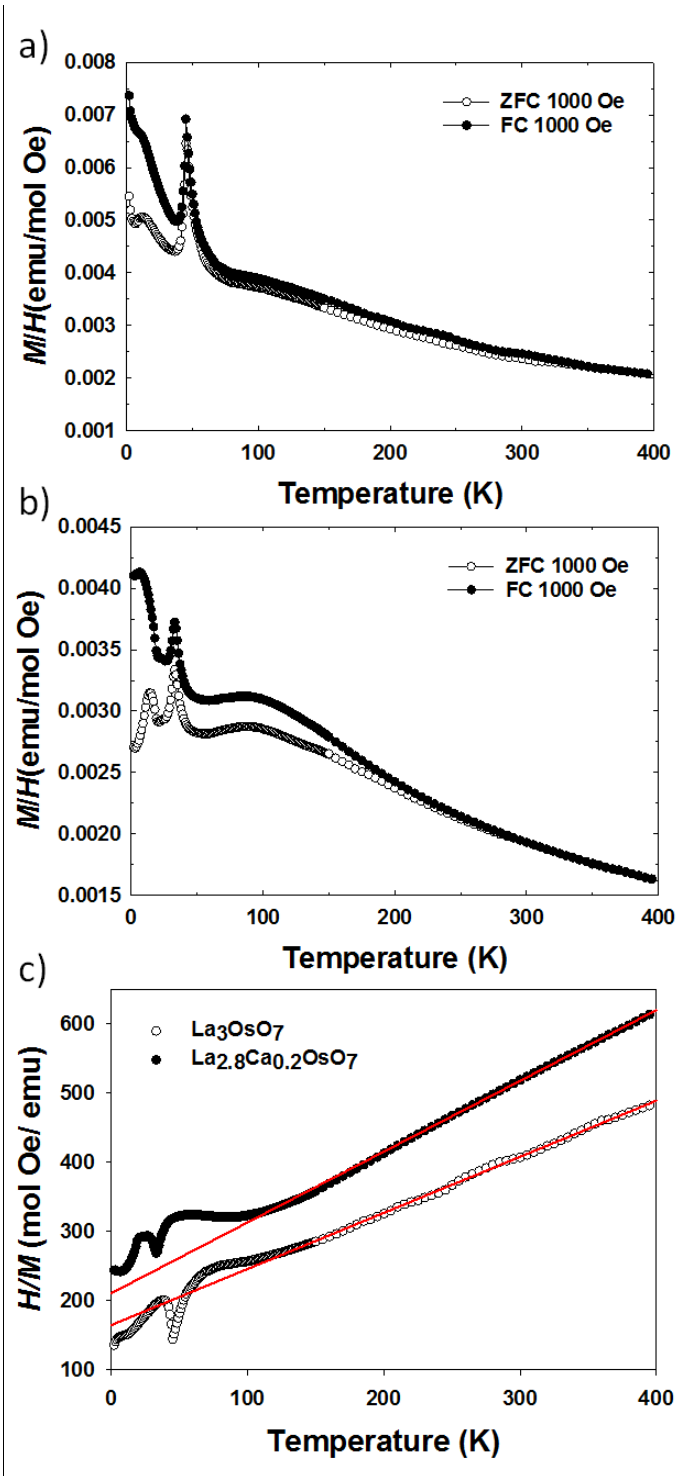

FIG. 4 (color online). The temperature dependence of the magnetization of (a) La_3OsO_7 and (b) $La_{2.8}Ca_{0.2}OsO_7$. The inverse relationship with Curie-Weiss fits (red lines) are shown in (c).

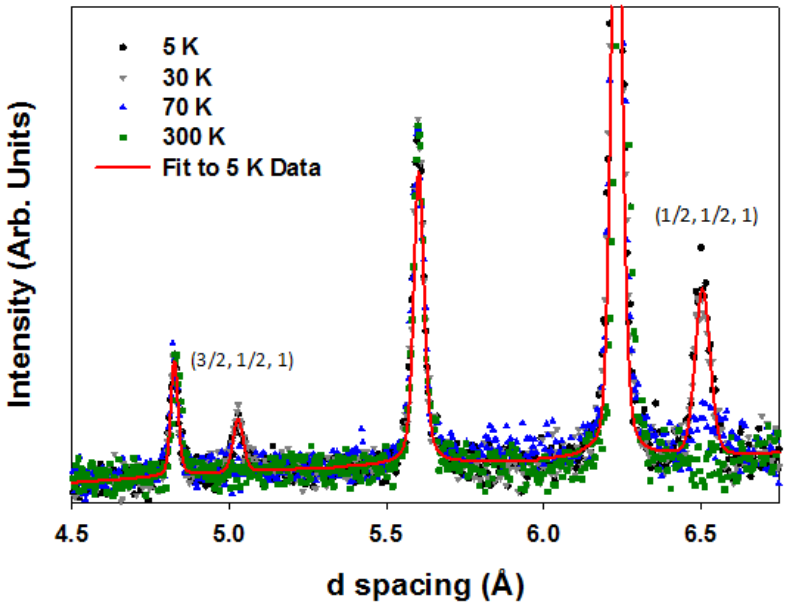

FIG. 5 (color online). High d-spacing neutron powder diffraction data showing the reflections arising due to magnetic scattering from La_3OsO_7. The calculated pattern including the magnetic model at 5 K is shown as the red curve.

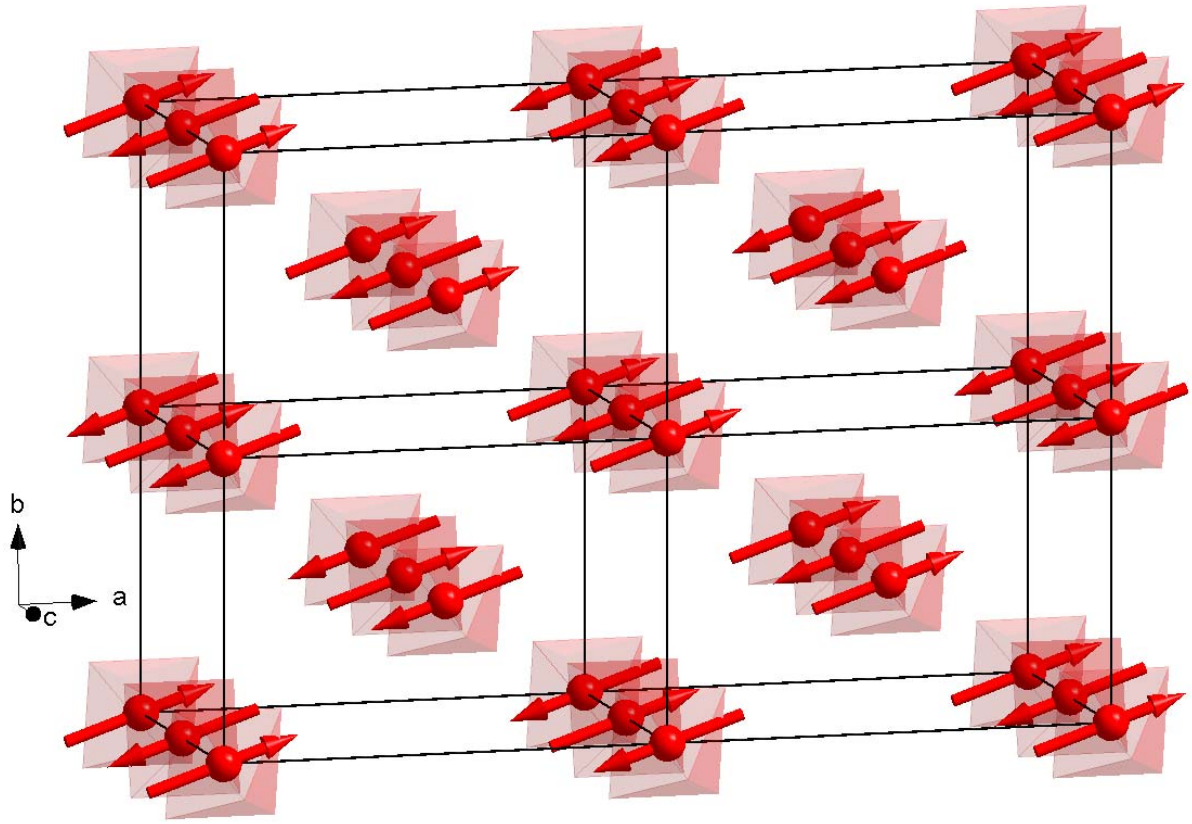

FIG. 6 (color online). Magnetic structure of La_3OsO_7 determined by analysis of neutron powder diffraction data shown on a 2 x 2 x 1 cell. The spins are coupled antiferromagnetically along each corner connected 1D chain of Os^{5+} octahedra down the *c* axis.

	La_3OsO_7			
	5 K	30 K	70 K	300 K
Space Group	*Cmcm*	*Cmcm*	*Cmcm*	*Cmcm*
a (Å)	11.1966(2)	11.1960(3)	11.1963(3)	11.2009(3)
b (Å)	7.4915(1)	7.4920(2)	7.4960(2)	7.5224(2)
c (Å)	7.6198(1)	7.6192(2)	7.6185(2)	7.6210(2)
V $(Å)^3$	639.15(1)	639.10(4)	639.41(5)	642.13(4)
R_{wp}	3.60%	3.64%	3.63%	3.29%
χ^2	2.864	2.928	2.918	2.449
Os-O1 (×2) (Å)	1.98812(2)	1.98728(4)	1.98823(4)	1.9907(4)
Os-O2 (×4) (Å)	1.96848(2)	1.96854(3)	1.96778(3)	1.963(1)
∠Os-O1-Os	146.739(1)	146.872(1)	146.653(1)	146.3 (1)
La2 x	0.2774(1)	0.2773(1)	0.2774(1)	0.2776(1)
La2 y	0.3119(2)	0.3121(2)	0.3121(2)	0.3118(2)
O1 y	0.4240(3)	0.4244(3)	0.4239(3)	0.4233(4)
O2 x	0.1239(1)	0.1238(1)	0.1240(1)	0.1234(1)
O2 y	0.1820(2)	0.1819(2)	0.1814(2)	0.1808(2)
O2 z	0.0403(2)	0.0405(2)	0.0405(2)	0.0404(2)
O3 x	0.3697(1)	0.3697(1)	0.3697(1)	0.3695(1)
O3 y	0.0317(2)	0.0315(2)	0.0315(2)	0.0314(2)
La1 U	0.0030(2)	0.0038(3)	0.0044(3)	0.0103(3)
La2 U	0.0015(2)	0.0017(2)	0.0021(2)	0.0053(2)
Os U	0.0015(2)	0.0014(2)	0.0020(2)	0.0042(2)
O1 U_{eq}	0.0041(5)	0.0035(5)	0.0037(5)	0.0072(6)
O2 U_{eq}	0.0062(3)	0.0066(3)	0.0073(3)	0.0147(4)
O3 U_{eq}	0.0033(3)	0.0034(4)	0.0035(4)	0.0063(4)
Os moment (μ_B)	1.7(1)	1.7(1)	-	-
Moment angle	21(7)	27(8)	-	-

TABLE 1 – Refinement parameters from neutron powder diffraction from La_3OsO_7. U_{eq} is defined as a third of the trace of the tensor for anisotropically refined U's, which are available in Ref. [32]. Moment angle is defined as the angle away from the *a* axis within the *ab* plane. Special positions used are La1 (0, 1/2, 0), La2 (x, y, 1/4), Os (0, 0, 0), O1 (1/2, y, 1/4), and O3 (x, y, 1/4).

	$La_{2.8}Ca_{0.2}OsO_7$				
	5 K	25 K	45 K	70 K	300 K
Space Group	*Cmcm*	*Cmcm*	*Cmcm*	*Cmcm*	*Cmcm*
a (Å)	11.1808(3)	11.1808(3)	11.1811(3)	11.1808(3)	11.1875(3)
b (Å)	7.4990(2)	7.4992(2)	7.5003(2)	7.5022(2)	7.5235(2)
c (Å)	7.6127(2)	7.6125(2)	7.6122(2)	7.6122(2)	7.6168(2)
V $(Å)^3$	638.29(4)	638.28(4)	638.37(4)	638.52(4)	641.10(4)
R_{wp}	4.23%	4.20%	4.16%	4.17%	3.81%
χ^2	3.420	3.450	3.386	3.446	2.913
Os-O1 (×2) (Å)	1.98783(5)	1.98765(5)	1.98791(5)	1.98784(5)	1.99131(4)
Os-O2 (×4) (Å)	1.96692(4)	1.96648(4)	1.96533(4)	1.96501(4)	1.96276(3)
∠Os-O1-Os	146.438(1)	146.460(1)	146.399(1)	146.409(1)	145.979(1)
La2 x	0.2774(1)	0.2773(1)	0.2774(1)	0.2773(1)	0.2778(1)
La2 y	0.3116(2)	0.3119(2)	0.3117(2)	0.3117(2)	0.3116(2)
O1 y	0.4235(4)	0.4235(4)	0.4234(4)	0.4234(4)	0.4226(4)
O2 x	0.1236(1)	0.1236(1)	0.1236(1)	0.1237(1)	0.1235(1)
O2 y	0.1820(3)	0.1819(2)	0.1817(2)	0.1815(2)	0.1808(2)
O2 z	0.0403(2)	0.0405(2)	0.0404(2)	0.0404(2)	0.0406(2)
O3 x	0.3695(2)	0.3694(2)	0.3696(2)	0.3694(2)	0.3693(2)
O3 y	0.0310(2)	0.0311(3)	0.0313(3)	0.0309(3)	0.0304(3)
La1 U	0.0052(3)	0.0050(3)	0.0052(3)	0.0061(3)	0.0103(4)
La2 U	0.0021(2)	0.0021(2)	0.0023(2)	0.0026(2)	0.0057(2)
Os U	0.0019(2)	0.0019(2)	0.0023(2)	0.0022(2)	0.0045(2)
O1 U_{eq}	0.0043(6)	0.0039(6)	0.0044(6)	0.0044(6)	0.0077(7)
O2 U_{eq}	0.0092(4)	0.0089(4)	0.0095(3)	0.0099(4)	0.0154(4)
O3 U_{eq}	0.0043(4)	0.0041(4)	0.0044(4)	0.0045(4)	0.0072(5)
Os moment (μ_B)	1.2(2)	1.3(2)	-	-	-
Moment angle	30(8)	31(9)	-	-	-

TABLE 2 – Refinement parameters from neutron powder diffraction from $La_{2.8}Ca_{0.2}OsO_7$. U_{eq} is defined as a third of the trace of the tensor for anisotropically refined U's, which are available in Ref. [32]. Moment angle is defined as the angle away from the *a* axis within the *ab* plane. Special positions used are La1 (0, 1/2, 0), La2 (x, y, 1/4), Os (0, 0, 0), O1 (1/2, y, 1/4), and O3 (x, y, 1/4).